applied sciences

MDPI

Article

The Effect of a Magnetic Field on the Transport of Functionalized Magnetite Nanoparticles into Yeast Cells

Bernadeta Dobosz [1,*], Eliza Gunia [1], Klaudia Kotarska [1], Grzegorz Schroeder [2] and Joanna Kurczewska [2]

[1] Faculty of Physics, Adam Mickiewicz University, Uniwersytetu Poznańskiego 2, 61-614 Poznan, Poland; eligun@st.amu.edu.pl (E.G.); klakot3@st.amu.edu.pl (K.K.)
[2] Faculty of Chemistry, Adam Mickiewicz University, Uniwersytetu Poznańskiego 8, 61-614 Poznan, Poland; schroede@amu.edu.pl (G.S.); asiaw@amu.edu.pl (J.K.)
* Correspondence: benia@amu.edu.pl

Abstract: Magnetic nanoparticles are of great interest to scientists as potential drug carriers. Therefore, it is essential to analyze the processes these nanoparticles undergo at the cellular level. The present paper demonstrates the effect of a constant and rotating magnetic field on penetration of TEMPOL-functionalized magnetite nanoparticles into yeast cells. The interactions between nanoparticles and yeast cells without and with a magnetic field were studied using electron spin resonance spectroscopy (ESR). The results showed that the ESR method can monitor the effect of a magnetic field on the magnetite nanoparticle penetration rate into the cells.

Keywords: magnetite nanoparticles; electron spin resonance; nanoparticles uptake; TEMPOL spin label; yeast cells; magnetic field

check for updates

Citation: Dobosz, B.; Gunia, E.; Kotarska, K.; Schroeder, G.; Kurczewska, J. The Effect of a Magnetic Field on the Transport of Functionalized Magnetite Nanoparticles into Yeast Cells. *Appl. Sci.* **2024**, *14*, 1343. https://doi.org/10.3390/app14041343

Academic Editors: Patrik Kamencay, Roman Radil and Jakub Misek

Received: 4 December 2023
Revised: 31 January 2024
Accepted: 2 February 2024
Published: 6 February 2024

1. Introduction

In medical sciences, magnetic nanoparticles can be applied in diagnostics and medical therapy [1]. As contrast agents in medical imaging, they can improve the quality of imaging and the sensitivity of diagnostic methods, such as magnetic resonance imaging (MRI) [2–6]. In magnetic hyperthermia, magnetic nanoparticles are used to support the destruction of cancer cells caused by heating [5,7,8]. However, their application as drug carriers seems to be the most promising [2,9,10]. The magnetic properties of such nanocarriers facilitate their targeting to the desired site and limit damage to healthy cells [10]. It also provides an opportunity to increase the effectiveness of treatment while reducing the therapeutic drug dose. All of the applications mentioned above result from the magnetic properties of nanoparticles, their biocompatibility, and sample stability. However, their potential toxicity to the body remains a challenge [10,11].

Targeted drug delivery, mostly promising in cancer treatment, by magnetic nanoplatforms is related to their interactions at the cellular level, i.e., attachment to the cell, the process of entering it, and its further behavior in the cell [12]. The methods currently used for analyzing interactions at the cell level include flow cytometry, different types of microscopy, and mass spectrometry [13–15]. However, these methods have significant limitations, and their applicability is related to specific particles and sensitivity, resolution, and availability, related to technical requirements. Alternatively, Krzyminiewski proposed using electron spin resonance (ESR) spectroscopy to monitor the endocytosis of nanomaterials functionalized with spin labels into cells [16,17]. Reactive oxygen species (ROS) are constantly produced in cells, and mitochondria are considered their primary endogenous source [18]. Based on the qualitative and quantitative changes in ESR signals from free radicals, the uptake of nanoparticles functionalized with spin labels in cells can be tracked.

ESR is a suitable and direct method for studying materials with unpaired electrons, including free radicals [19,20]. In general, after placing the sample in a magnetic field, the Zeeman effect occurs, which involves splitting the energy levels of the unpaired electron.

If the resonance condition is met and an appropriate quantum of radiation with energy corresponding to the energy difference between these levels is supplied to the system, the ESR phenomenon will be registered as the first derivative of the absorption signal [19–21]. It has been successfully applied in various studies, including those investigating the properties of magnetic nanoparticles [22–27], iron complexes and free radicals in blood and tissues [28–35], as well as geological and archaeological materials [36–39]. ESR studies confirm the penetration of nanoparticles into cells and facilitate monitoring of this whole process. Additionally, magnetic nanoparticles with attached spin labels (TEMPO or TEMPOL), as potential antioxidant agents, have been investigated for their possible use in treating inflammatory diseases, as radioprotectors in radiotherapy, and scavengers of free radicals in cells [17,32,40,41].

As standard, both TEMPO and TEMPOL are used as spin probes in ESR studies [18,42] due to the presence of stable unpaired electrons. They are applied in biological and medical research with cells and membranes. Because of the possibility of reaction with free radicals, including ROS, they are also studied as potential antioxidants and oxidative stress-reducing agents. For example, Mołoń et al. [42] studied the influence of TEMPO on yeast cells, considering their physiology, aging, and gene expression changes. Its antioxidant properties were checked by various methods without ESR. On the other hand, Nagasaki's group [18,41,43] used TEMPO and TEMPOL in micelle-type nanoparticles for disease treatment, including chemo- and radiotherapy of cancer. In other studies, TEMPO was applied as a redox-sensitive MRI contrast agent, and the effects of TEMPO-type nitroxides on ascorbate reduction were tested [44,45]. The cell membrane acts as a barrier separating the interior of the cell from its external environment. It regulates ion and particle flow to a cell [46,47]. The particles can interact with the membrane and then pass through by endocytosis and direct permeation, but the former dominates in the interactions between nanoparticles and cells [48]. The manner of nanoparticle internalization depends on its size and shape, surface charge, and topography. An important feature is surface functionalization [12,49]. Depending on the size, endocytosis is divided into two types: phagocytosis, during which the uptake of large particles (>500 nm) occurs, and pinocytosis, which includes different mechanisms such as macropinocitosis, clathrin/caveolin-mediated endocytosis, and clathrin/caveolin independent endocytosis.

The magnetic field is considered a factor that influences the endocytosis process. Its role has been studied and described in the literature for its effects on cell functions and the transport of magnetic nanoparticles to targeted cells and tissues [50–52]. Zablotskii et al. described the effect of a high-gradient magnetic field on cell life [53]. They observed that a magnetic field of about 1 T with a gradient of up to 1 GT/m can significantly affect cells. Similarly, in studies concerning prostate cancer cells and human macrophages, the presence of a high gradient magnetic field increased the internalization of superparamagnetic iron oxide nanoparticles [54,55]. Additionally, Uzhytchak et al. [56] observed that the application of a high intensity (7 T) pulsed magnetic field increases the uptake of superparamagnetic iron oxide nanoparticles through the cell membrane.

The literature also analyzes the influence of magnetic fields on reactive oxygen species (ROS) [57]. These are highly reactive free radicals, capable of disrupting cell function and initiating various diseases, including cancer. The impact of various types of magnetic field on human and animal cells is described in the literature [57]. Generally, a magnetic field increases ROS concentrations in cells and tissues, but there are exceptions to this rule. The effect depends on the type of magnetic field applied, its intensity, exposure time, frequency, and the kind of biological samples studied. The research conducted with magnetic fields, biological materials, and drug-functionalized magnetic nanoparticles can contribute to clinical applications, especially for ROS-related diseases. Therefore, we propose applying the ESR method as a suitable technique for the combined study of the influence of a magnetic field on the uptake of magnetic nanoparticles by cells and the concentration of free radicals within them.

Yeast cells are used as a model in several studies to analyze processes similar to these in human cells [58,59]. Van der Laan et al. [58] characterized the oxidative stress in yeast cells after internalizing fluorescent nanodiamonds proposed as free radical biosensors. Eigenfeld et al. [60] described the impact of nanoparticles on yeast cell viability and Mołoń [42] reported the antioxidant properties and toxic effect of the TEMPO spin label. Yeast cells were also applied under various cellular stress impacts, including oxidative, osmotic, and ethanol accumulation [59]. In turn, Krzyminiewski and Dobosz applied yeast cells in the study of magnetic nanoparticle uptake and the antioxidant properties of a TEMPO spin probe using ESR [16,17,32].

This study aimed to investigate the effect of a magnetic field on the transport of TEMPOL-functionalized magnetite nanoparticles into yeast cells by ESR spectroscopy.

2. Materials and Methods

2.1. Materials

(3-Glycidoxypropyl)trimethoxysilane (GPTMS), 1,8-diazabicyclo[5.4.0]undec-7-ene (DBU), 4-hydroxy-2,2,6,6-tetramethylpiperidine-1-oxyl (TEMPOL), $FeCl_3 \bullet 6H_2O$, and $FeCl_2 \bullet 4H_2O$ were purchased from Merck Sigma-Aldrich (Saint Louis, MO, USA). Additional chemicals comprised analytic grade reagents that were commercially obtainable and employed without additional purification steps. Demineralized water was used to prepare aqueous solutions.

2.1.1. Synthesis Procedure

Iron (II, III) oxide nanoparticles were synthesized using standard co-precipitation of ferric and ferrous ions under basic conditions [61,62]. The Fe_3O_4 nanopowder was subsequently used for functionalization with (3-glycidoxypropyl)trimethoxysilane (GPTMS). For this purpose, 20 mL of water was added to 100 mg of Fe_3O_4. Subsequently, 1 g of citric acid was dissolved in 10 mL of water and introduced into the aforementioned solution, where it was stirred for 2 h. Finally, the solution underwent sonication for 5 min to achieve a stable suspension. Simultaneously, a pre-hydrolyzed GPTMS solution was created by combining 10 mL of water and tetrahydrofuran (THF) mixture with 107 mg of GPTMS, followed by stirring for 1 h [63]. Then, 1 mL of the prepared solution was added to 20 mL of the previously prepared suspension and stirred constantly for 6 h. The nanoparticles functionalized with GPTMS underwent magnetic separation and were subsequently rinsed three times with distilled water. Finally, the glycidoxypropyl-functionalized magnetite nanoparticles (Fe_3O_4@GLY) were dried under vacuum for 16 h at 50 °C.

A portion of Fe_3O_4@GLY nanoparticles was used for the synthesis of TEMPOL-functionalized magnetite. For this purpose, 20 mL of THF was added to 100 mg of Fe_3O_4@GLY. Then, 30 mg of TEMPOL and 5 mg of the strong base, 1,8-diazabicyclo[5.4.0]undec-7-ene (DBU), were added. The suspension was stirred for 5 h. The final product, Fe_3O_4@TEMPOL nanoparticles, underwent magnetic separation and were rinsed with THF three times. Subsequently, the magnetic nanoparticles were dried under vacuum conditions.

2.1.2. Yeast Cells Preparation

Bakery yeast (*Saccharomyces cerevisiae*) (1 g) was diluted in 50 mL of distilled water with 0.3 g sucrose. Such solution was incubated at 37 °C for 1 h. After this time, 1.5 mL of the suspension of Fe_3O_4@TEMPOL nanoparticles (concentration 0.5 gL^{-1}) was added to 1 mL of yeast cells, and the incubation was continued. Every 45 min, samples of the solution were taken for ESR measurements.

2.2. Methods

2.2.1. Nanoparticles Characterization

X-ray diffraction (XRD) measurements were performed using a Bruker AXS D8 Advance powder diffractometer (Karlsruhe, Germany) equipped with a Johansson monochromator (λCu $K_{\alpha 1}$ = 1.5406 Å). The particle size was analyzed using a Joel ARM 200F transmission electron microscope (Peabody, MA, USA). The thermogravimetric studies

were carried out using a Setarm Setsys 1200 apparatus (Caluire, France). The curves were recorded at a heating rate of 10 °C min^{-1} under a helium atmosphere.

2.2.2. ESR Measurements

ESR measurements were made using an X-band EMX-10 spectrometer from Bruker (Bruker Co., Billerica, MA, USA). The magnetic field modulation frequency was 100 kHz. The samples were measured in Pasteur pipettes. The measurements were conducted at 260 K to assess whether nanoparticles can enter cells at specific nanoparticle/cell ratios (magnetic sweep width of 13 mT, modulation amplitude of 0.2 mT). The temperature during the measurements was controlled using a Bruker temperature controller unit (ER 4131VT). Then, the samples were measured at 295 K (magnetic sweep width of 8 mT, modulation amplitude of 0.01 mT). The spectrometer was operating with the following settings: microwave power of 7.97 mW, sweep time of 41.9 s, conversion time of 40.96 ms, and the time constant was 40.96 ms. The concentration of free radicals in the studied samples was calculated from the integrated intensity of ESR signals from the attached TEMPOL spin label with an accuracy of 5%. All ESR experiments were repeated three times.

2.2.3. The Impact of a Stable Magnetic Field on Nanoparticle Uptake by Yeast Cells

Two experiments were conducted to examine the impact of a magnetic field on the interactions between magnetite nanoparticles and yeast cells. In the first one, a neodymium magnet with a magnetic induction of 440 mT on the surface (about 5 mT on the edge of the glassware) and a diameter of 6 mm was used (Figure 1). The Petri dish (diameter 30 mm) with the sample was incubated on the magnet. Analogous conditions were applied to the control sample not exposed to a magnetic field. Each time, three measurements were taken: the focusing point, the edge of the glassware, and a control sample.

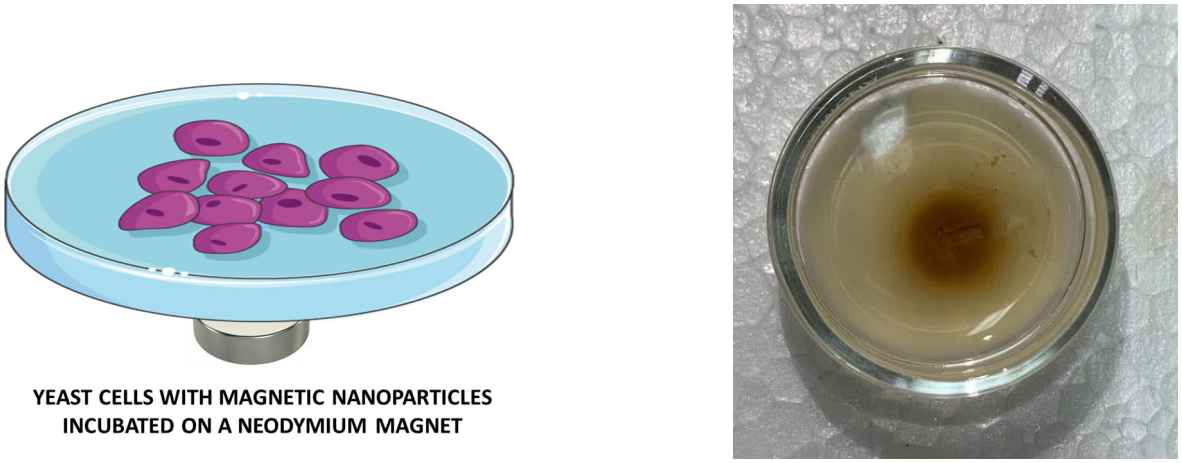

(**a**) (**b**)

Figure 1. Experiment with a neodymium magnet: (**a**) Petri dish with yeast cells and magnetite nanoparticles placed on a neodymium magnet; (**b**) digital photograph taken during the experiment. The figure was created using Servier Medical Art templates, licensed under a Creative Commons Attribution 3.0 Unported License; https://smart.servier.com (accessed on 20 November 2023).

2.2.4. The Impact of a Rotating Magnetic Field on Nanoparticle Uptake by Yeast Cells

In the subsequent experiment, equipment for magnetic nanoparticle focusing in three-dimensional space (MNF-3D) was used as the source of a rotating magnetic field (Figure 2) [64–66]. The magnetic field values inside the rotation center were about 22 mT and 12 mT on the edge of the glassware. The diameter of the Petri dish with the sample was 40 mm. The experiment was conducted in two stages. The first stage was focused on investigating the influence of a rotating magnetic field on the entry of magnetite nanoparticles into yeast cells. The samples were placed in the rotating magnetic field for 15 min

and 30 min, respectively. Subsequently, the samples were incubated, and their signals were measured by the electron spin resonance (ESR) method until their disappearance. An analogous procedure was applied to the control sample. In the second stage, the sample was incubated, and directly before ESR measurement, it was placed in a rotating magnetic field for 15 min. The measurements were taken for the focusing point, the edge of the Petri dish, and a control sample.

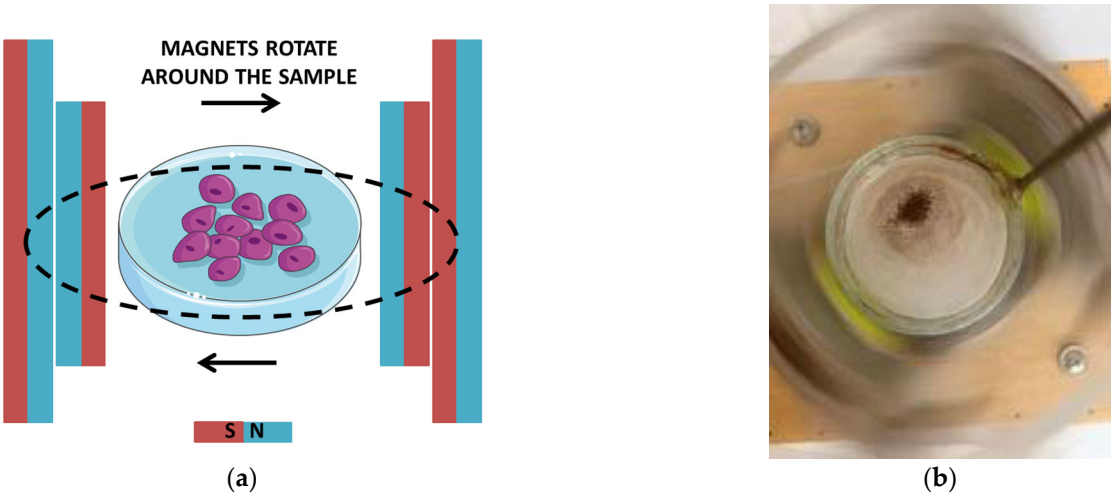

(**a**) (**b**)

Figure 2. Experiment with MNF-3D: (**a**) Scheme with the equipment generating a rotating magnetic field; (**b**) digital photograph taken during the experiment. (Two magnets with a magnetic induction of 60 mT and a diameter of 70 mm and two others with a diameter of 35 mm and magnetic induction of 30 mT). The figure was created using Servier Medical Art templates, licensed under a Creative Commons Attribution 3.0 Unported License; https://smart.servier.com (accessed on 20 November 2023).

2.2.5. Microscopic Observation of Yeast Cell Proliferation

Additionally, an optical microscope was used to control the number of yeast cells in each experiment. Three pictures were taken for each sample, and the number of cells was calculated using Image J, a Java-based image processing program. The results were analyzed separately for individual experiments.

2.2.6. SEM and EDS of Yeast Cells with Fe_3O_4@TEMPOL Nanoparticles

After 45 min of yeast cell incubation with Fe_3O_4@TEMPOL nanoparticles, the sample for scanning electron microscopy (SEM) was prepared following the protocol for cultured microorganisms. Briefly, medium containing yeast cells was centrifuged. Then, the pellet was resuspended in 5% glutaraldehyde solution (phosphate-buffered saline (PBS), pH 7.4) and left for 1 h. Subsequently, the sample was centrifuged and washed twice with PBS solution. Finally, the yeast cells were dehydrated using an increasing ethanol gradient (30, 50, 70, and 100%) and dried overnight. Finally, the sample was covered with a thin layer of gold and analyzed using a scanning electron microscope (SEM, SU3500) fitted with an energy-dispersive (EDS) detector for elemental analysis (Hitachi, Tokyo, Japan).

2.2.7. Statistical Analysis

ESR measurement data are shown as the mean value ± 5% accuracy, and optical microscopic observation data are shown as the mean value ± standard deviation (SD). A one-way ANOVA test with a significance level defined as 0.05 was applied in the statistical analysis of free radical concentrations and yeast cell proliferation.

3. Results and Discussion

The material studied, Fe_3O_4@TEMPOL, was initially characterized using physicochemical methods (Figure 3). The XRD pattern of magnetite was confirmed by reflections at 2 theta: 29.7, 35.1, 42.4, 53.8, 57.6, and 65.1 (Joint Committee for Powder Diffraction Studies, JCPDS No. 74-0748). The diffraction reflections associated with Fe_3O_4 were also observed in Fe_3O_4@GLY and Fe_3O_4@TEMPOL samples. This confirmed the stability of the magnetite structure during the organic functionalization of its surface. TEM images indicated irregular shapes of nanoparticles with average sizes ranging from 10 to 20 nm. The presence of an organic layer was confirmed by thermogravimetric measurement. Pure magnetite and the nanoparticles with organic units already demonstrated initial weight losses (1%) below 120 °C due to adsorbed water molecules. However, the decomposition of organic units resulted in an increased weight loss at 200–400 °C compared to the initial Fe_3O_4. Notably, the total mass loss for Fe_3O_4@TEMPOL was slightly greater than that for Fe_3O_4@GLY, suggesting an increase in the organic layer on the magnetite surface. In the next step, the presence of TEMPOL on the magnetite surface was confirmed by electron spin resonance (ESR) spectroscopy.

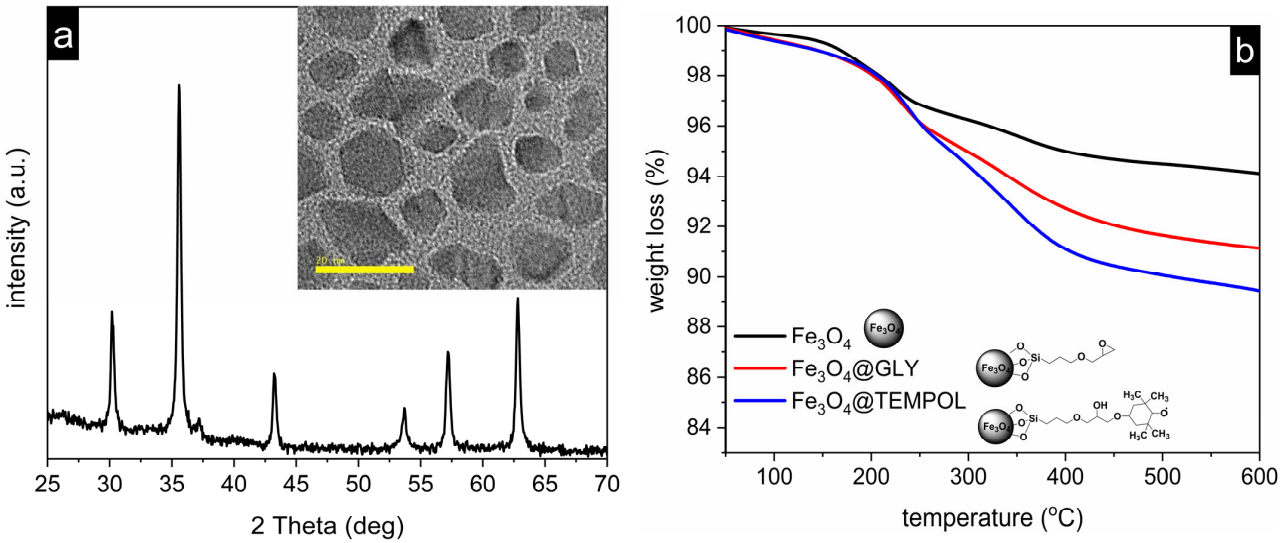

Figure 3. (**a**) XRD pattern and TEM image (inset) of Fe_3O_4 nanoparticles; (**b**) thermogravimetric curves of Fe_3O_4, Fe_3O_4@GLY, and Fe_3O_4@TEMPOL.

In previous papers, we showed the application of the ESR method to monitor the uptake of functionalized magnetite nanoparticles by yeast cells and cancer cells [16,17]. These pilot studies concentrated on the effect of a magnetic field on the course of this process. Figure 4a,b show a typical ESR spectrum of magnetite nanoparticles recorded at a temperature of 260 K. The broad line (Figure 4a) corresponds to the magnetic core and the narrow one to the TEMPOL spin label attached to the surface of the nanoparticles. This line is in fact a triplet, resulting from the hyperfine interaction of the spin of the unpaired electron with the spin of the nitrogen nucleus (Figure 4b). Figure 4c,d demonstrate the spectra of nanoparticles and TEMPOL attached to them, recorded at 295 K. The ESR signal from the TEMPOL spin label recorded at low temperature (Figure 4b) was taken to observe the interactions between nanoparticles and cells and the uptake of nanoparticles. According to our previous results, such a spectrum consisting of three lines obtained in the frozen sample indicated the penetration of nanoparticles into cells [16,17,32].

The next research step concerned the influence of the magnetic field generated by a neodymium magnet on the magnetic nanoparticle penetration rate into cells (Figure 1). The results are shown in Figure 5. The concentration of free radicals in the sample during the incubation decreased due to reactions with radicals and reactive oxygen species, which probably occur in cellular mitochondria. As a result of such redox reactions, the attached

spin label was reduced to stable hydroxylamines [17,32]. Importantly, the control and the sample incubated in a magnetic field behaved differently (Figure 5). In the case of the control sample, the concentration of free radicals in subsequent measurements was lower than that in the sample incubated in the presence of the magnetic field. Moreover, the signal decayed earlier in the control sample. It can, therefore, be concluded that incubation of the sample in a constant magnetic field slowed down the interactions between nanoparticles and cells. The results were statistically significantly different for the defined significance level of 0.05. A similar relationship has been described in the literature [51]. The authors studied the effect of a pulsed magnetic field and compared the results for a constant magnetic field. It was found that, in a constant magnetic field, the transport of magnetic nanoparticles across cells was slower. Furthermore, their microscopic observations revealed that, under a constant magnetic field, this transportation was hindered by the formation of large aggregates of nanoparticles. These aggregates, owing to their size, were unable to undergo endocytosis. Also, Soheilian et al. [52] discovered that using very strong magnetic fields to deliver nanoparticle-based drugs caused their aggregation within minutes to sizes exceeding the size of intercellular pores in cancer tissues, thus preventing them from reaching their target sites. Since, in our study, the samples were always stable on the magnet (there was no movement), the nanoparticles could accumulate in the form of larger aggregates on the magnet.

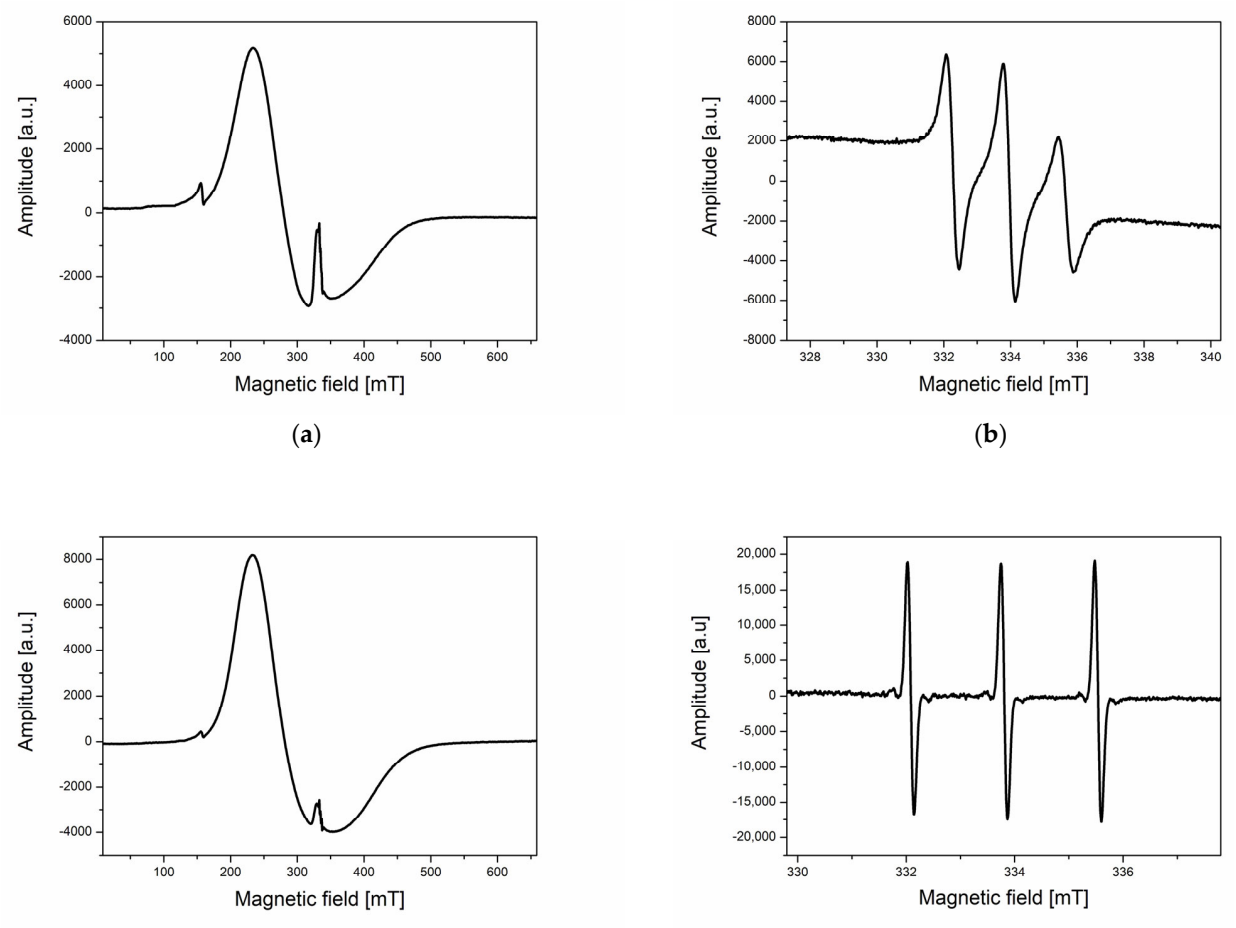

Figure 4. Representative ESR spectra of TEMPOL-functionalized magnetite nanoparticles with yeast cells: (**a**) Magnetite core with TEMPOL recorded at 260 K, magnetic sweep width of 650 mT; (**b**) signal from attached TEMPOL recorded at 260 K, magnetic sweep width of 13 mT; (**c**) magnetite core with TEMPOL recorded at 295 K, magnetic sweep width of 650 mT; (**d**) signal from attached TEMPOL recorded at 295 K, magnetic sweep width of 8 mT.

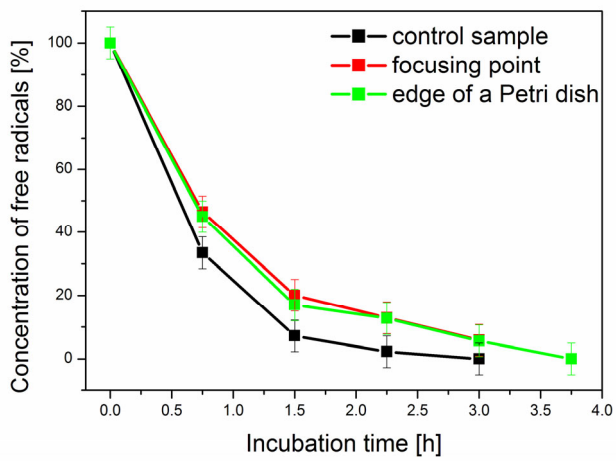

Figure 5. Decrease in free radical concentration with time after incubation of yeast cells with TEMPOL-functionalized magnetite nanoparticles without a magnetic field (control sample) and on a neodymium magnet (red line for samples taken from the focusing point and green line from the edge of a Petri dish). The data for each point are shown as the mean value ± 5% of ESR accuracy. The results exhibit statistically significant differences (one-way ANOVA test, significance level 0.05).

In the second experiment, we applied a rotating magnetic field to check its impact on magnetic nanoparticle uptake by cells using the previously designed apparatus for nanoparticle focusing (Figure 2) [64–66]. The results are shown in Figure 6. In the first part of the experiment (Figure 6a), samples were kept in a rotating magnetic field for the appropriate time and then incubated. For the significance level of 0.05, the results were statistically significantly different for the measurements performed after 1.5 and 2.25 h (3 and 4 points in the graph). However, the general tendency was similar to the results observed in the experiment with the neodymium magnet (Figure 5). In this experiment, the samples were incubated after exposure to a rotating magnetic field and measured at subsequent time intervals. Moreover, the induction of the magnetic field used in this case was only 22 mT in the center of the Petri dish with the sample and 11 mT at its edge.

An opposite tendency was observed in the second stage of this experiment (Figure 6b). The concentration of free radicals decreased faster in the sample exposed to a rotating magnetic field just before the measurement compared to the control sample. Such changes can probably be connected with the prolonged production of reactive oxygen species (ROS) in cells caused by a magnetic field [50]. For the significance level of 0.05, the results were statistically significantly different for the measurements performed after 0.75 h and 1.5 h (2 and 3 points in the graph). The effect of a rotating magnetic field on cancer cells was studied by Sharpe et al. [67]. An electromagnetic field increases the reactive oxygen species (ROS) level in cells. Additionally, a weak magnetic field can impact spin pairing with redox-active radicals. Thus, it may disrupt the flow of electrons in the mitochondrial electron transport chain. This could explain the faster decay of the ESR signal in the samples exposed to the rotating field in our experiment. The differences between the obtained results were not as apparent as in the case of the experiment with the neodymium magnet because the magnetic field induction was also much lower.

The number of yeast cells was controlled with an optical microscope during the experiments. The results are shown in Tables 1 and 2. Magnetic nanoparticles and a magnetic field had a negligible effect on cell number, with two exceptions marked in Table 2 without a statistical significance at the defined significance level of 0.05. The biological effects caused by low-frequency electromagnetic fields on yeast cells have been studied by Sladicekova et al. [68]. The authors exposed yeast cells to the magnetic field for 8 h and observed an inhibitory effect on cell growth and multiplication. In our studies, we limited cell observations to less than 4 h because the ESR signal disappeared after that. The purpose of our research was also not to verify the influence of a magnetic field on

biological effects in yeast cells. In the future, microscopic observations could be repeated by extending the time and changing the culture conditions with additional biological tests.

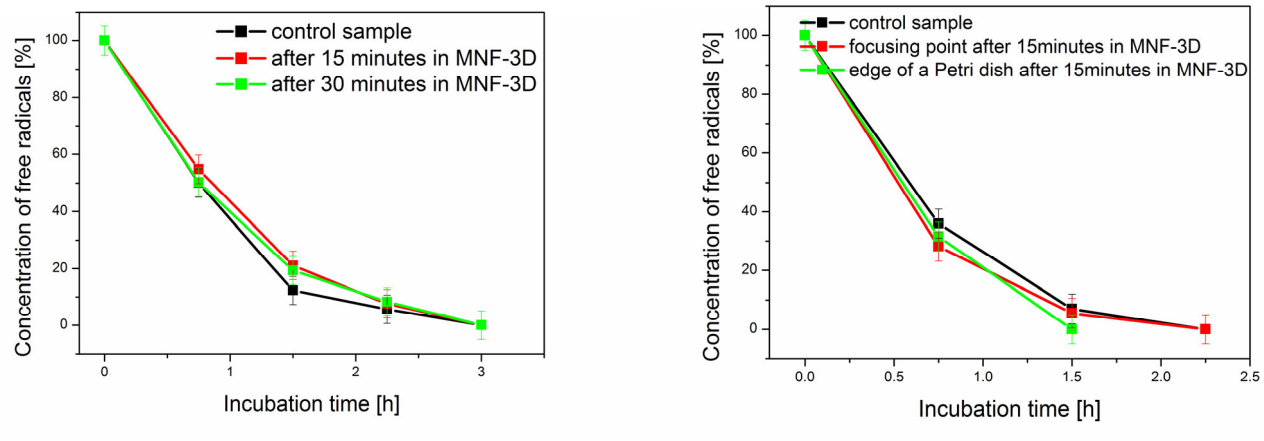

(**a**) (**b**)

Figure 6. Decrease in free radical concentration with time after incubation of yeast cells with TEMPOL functionalized magnetite nanoparticles incubated without a magnetic field (control sample): (**a**) samples kept in a rotating magnetic field for 15 and 30 min; (**b**) samples kept in a rotating magnetic field for 15 min. The data for each point are shown as the mean value ± 5% of ESR accuracy. The results exhibit statistically significant differences after 1.5 h and 2.25 h (**a**), and 0.75 h and 1.5 h (**b**) (one-way ANOVA test, significance level 0.05).

Table 1. The number of yeast cells in individual samples for the experiment with a neodymium magnet (mean value ± SD).

Time (h)	Control Sample (×10^6/mL)	YC + MNPs [1] (×10^6/mL)	YC + MNPs + NM [2] (×10^6/mL)
0 [N]	305 ± 46	255 ± 38	282 ± 42
0.75 [N]	349 ± 52	327 ± 49	262 ± 39
1.5 [N]	355 ± 53	274 ± 41	373 ± 56
2.25 [N]	269 ± 40	390 ± 59	383 ± 58
3 [N]	343 ± 52	380 ± 57	363 ± 55
3.75 [N]	326 ± 49	385 ± 58	339 ± 51

[1] Yeast cells with TEMPOL-functionalized magnetite nanoparticles. [2] Yeast cells with TEMPOL-functionalized magnetite nanoparticles incubated with a neodymium magnet. [Y] or [N]: statistically significant or not.

Table 2. The number of yeast cells in individual samples for the experiment with a rotating magnetic field (mean value ± SD).

Time (h)	Control Sample (×10^6/mL)	YC + MNPs [1] (×10^6/mL)	YC + MNPs + 15 [2] (×10^6/mL)	YC + MNPs + 30 [3] (×10^6/mL)
0 [N]	359 ± 54	332 ± 49	336 ± 50	270 ± 40
0.75 [Y]	354 ± 53	424 ± 64	271 ± 41	273 ± 40
1.5 [Y]	391 ± 59	396 ± 59	396 ± 61	260 ± 39
2.25 [N]	332 ± 50	360 ± 54	332 ± 50	322 ± 48
3 [N]	400 ± 60	352 ± 53	357 ± 54	347 ± 52
3.75 [N]	376 ± 56	321 ± 48	452 ± 68	340 ± 51

[1] Yeast cells with TEMPOL-functionalized magnetite nanoparticles. [2] Yeast cells with TEMPOL-functionalized magnetite nanoparticles kept in a rotating magnetic field during 15 min before incubation. [3] Yeast cells with TEMPOL functionalized magnetite nanoparticles kept in a rotating magnetic field during 30 min before incubation. [Y] or [N]: statistically significant or not.

The toxic effects of nanoparticles, including iron oxide nanoparticles, are described in the literature [60]. The studies cover both mammalian cells and yeast cells. In the study with yeast cells, uncoated nanoparticles were used, and mainly no negative impact on cell growth was observed. However, there are also studies in which the negative effects of such nanoparticles on yeast cell viability, apoptosis, and ROS generation were noticed. Due to the potential use of iron oxide nanoparticles, among others, in medicine, it is essential to investigate their toxic effects, both functionalized and unfunctionalized, on cells.

Yeast cells were also used to study the toxic effect of the TEMPO spin label [42]. The authors examined both the effect of TEMPO concentration (0.1 mM, 0.5 mM, 1 mM, 3 mM, and 5 mM) and incubation time of cells with the radical. It was observed that TEMPO at high concentrations (3 mM and 5 mM) inhibited the growth rate of yeast cells. In the second stage, for a concentration of 3 mM, the incubation time of cells with the radical was examined. The studies showed that a longer incubation time and higher concentration of the radical had an inhibitory effect on the growth of the tested cells. On the other hand, the described studies also confirmed the antioxidant properties of TEMPO [32,41,43].

Eigenfeld et al. [60] measured the impact of bare iron oxide nanoparticles on yeast cell viability. For two concentrations of nanoparticles (0.1 gL^{-1} and 1 gl^{-1}) and two strains of yeast cells, no significant impact within 6 h was observed. After 24 h, in one of the strains for the concentration of 1 gL^{-1}, a slightly negative effect (5%) on their viability was noticed. Our study used a low concentration of TEMPOL-functionalized magnetite nanoparticles (0.5 gL^{-1}) to eliminate their potential toxic effect on cells. However, the present study aimed to show the impact of a magnetic field on iron oxide nanoparticle uptake by yeast cells and the application of ESR to investigate this process.

The functionalized Fe_3O_4 nanoparticles possessed three distinct regions that facilitated accomplishing the research goals. The magnetite core, Fe_3O_4, rendered the molecule magnetically responsive, while the silica layer shielded Fe_3O_4 from external factors. Furthermore, the organic functional groups of silane facilitated the creation of robust hydrogen bonds with -OH, -NH, and COOH groups present on the cell surface, promoting the interaction of the magnetic NP with the cell surface. Finally, a spin label with oxidizing and radical-scavenging properties enabled rapid monitoring of the binding process of the magnetic nanoparticles in solution by recording ESR spectra. Detailed examinations of the molecular-level interactions between Fe_3O_4 particles without silica coating and yeast cells were conducted by Peng [69] [70] and Eigenfeld [60]. Conversely, investigations of the interactions between spin labels and cells were carried out by Pahlevan [70] and Mołoń [42].

Additionally, SEM images were captured and EDS analysis was performed for yeast cells incubated in the presence of Fe_3O_4@TEMPOL. In the SEM image obtained at the beginning of the incubation (Figure 7), the predominant findings involved yeast cells featuring functionalized magnetite nanoparticles on their surfaces, along with a minority of yeast cells existing independently without Fe_3O_4. Furthermore, there were a few observed aggregates of Fe_3O_4@TEMPOL that were not linked to yeast cells within the field of view. Yeast cells displayed attachment of the functionalized Fe_3O_4 nanoparticles on their surfaces at various locations. Nevertheless, the individual binding of single nanoparticles by yeast cells was not observed.

In order to determine the elemental composition of the selected yeast cells, EDS measurements were performed (Figure 8). Yeast cells without and those containing Fe_3O_4@TEMPOL were chosen for investigation. The elemental distribution obtained in both instances affirmed the binding of magnetite to the yeast cell surface, marked by a substantial increase in signals for Fe and O and the emergence of a signal for Si.

Studies on the influence of a magnetic field, both in terms of its impact on cell function and drugs attached to magnetic nanoparticles for delivery, have been described in the literature [32,50,51,53,68,71]. Indeed, the intersection of nanotechnology, medicine, and external influences like magnetic fields holds significant promise and raises intriguing questions about the potential use of magnetic nanoparticles functionalized with drugs and

participation of the magnetic field in medical diagnostics or treatment processes. Thus, this research holds immense importance and warrants continuous exploration.

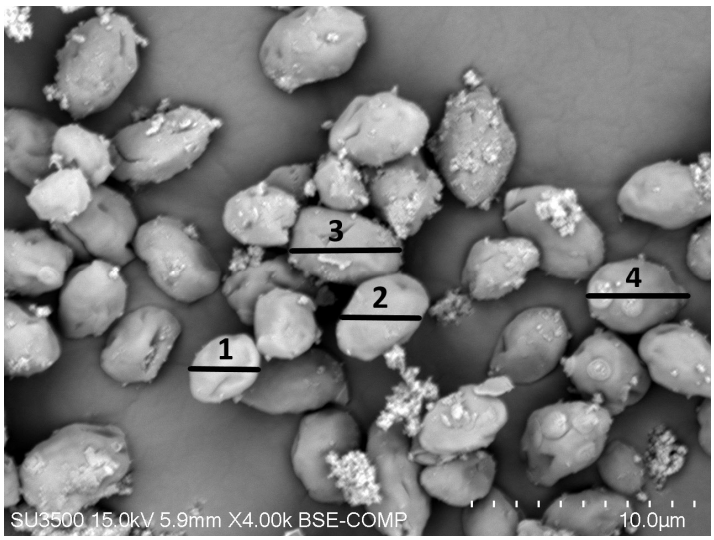

Figure 7. SEM image of yeast cells incubated with Fe_3O_4@TEMPOL.

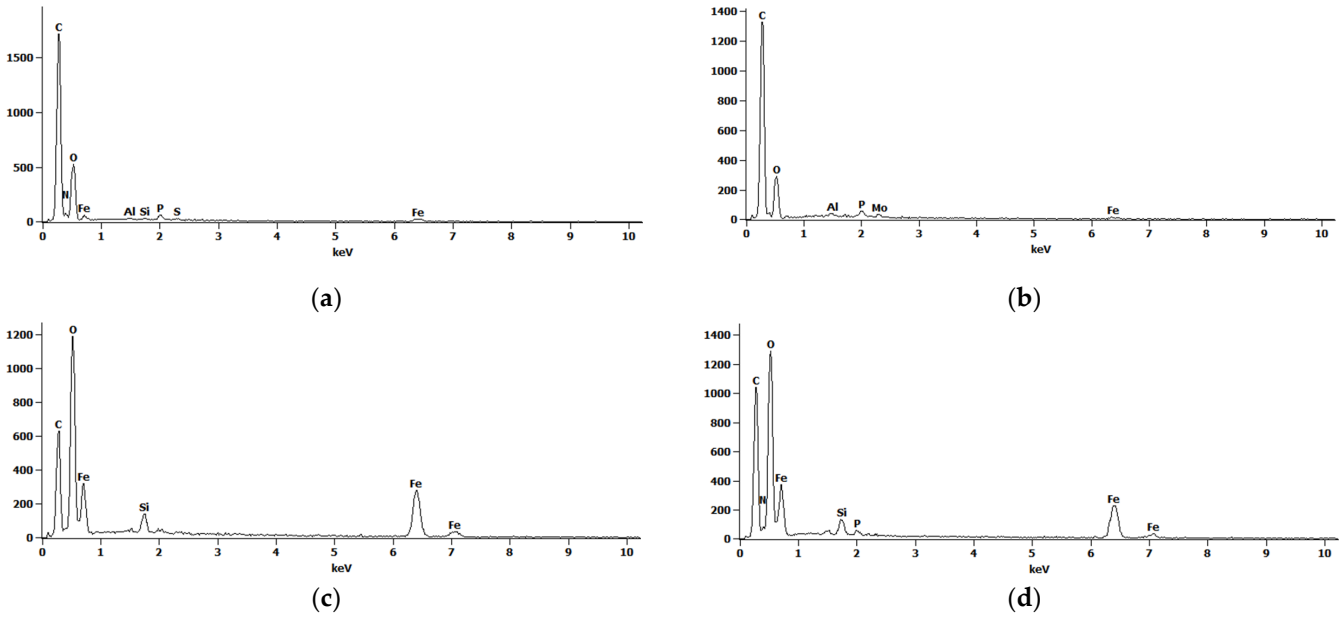

Figure 8. The results of EDS measurements for yeast cells marked in Figure 7: (**a**) cell 1; (**b**) cell 2; (**c**) cell 3; (**d**) cell 4.

4. Conclusions

ESR spectroscopy enables the study of the uptake of spin label-functionalized magnetite nanoparticles in cells and free radical reactions occurring inside cells. The present study showed that a magnetic field affects yeast cells with functionalized iron (II,III) oxide. The impact may concern cellular uptake, cytotoxicity, or oxidative stress. Considering the use of magnetic nanoparticles as potential drug carriers and magnetic fields in diagnostics and medical therapy, this research requires continuation for a more in-depth and comprehensive understanding of the complex processes occurring in cells in the presence of nanoparticles and a magnetic field.

Author Contributions: Conceptualization, B.D.; methodology, B.D., G.S., and J.K.; formal analysis, B.D., E.G., K.K., J.K., and G.S.; investigation, B.D., E.G., K.K., J.K., and G.S.; resources, B.D. and J.K.; data curation, B.D., E.G., K.K., J.K., and G.S.; writing—original draft preparation, B.D. and J.K.; writing—review and editing, B.D., G.S., and J.K.; visualization, B.D., E.G., K.K., and J.K.; supervision, B.D.; project administration, B.D.; funding acquisition, B.D. and J.K. All authors have read and agreed to the published version of the manuscript.

Funding: The study was financial supported by the interfaculty project at AMU School of Exact Sciences.

Institutional Review Board Statement: Not applicable.

Informed Consent Statement: Not applicable.

Data Availability Statement: Data supporting the results of our study are available from the corresponding author upon request.

Conflicts of Interest: The authors declare no conflicts of interest.

References

1. Benguettat-El Mokhtari, I.; Schmool, D.S. Ferromagnetic Resonance in Magnetic Oxide Nanoparticules: A Short Review of Theory and Experiment. *Magnetochemistry* **2023**, *9*, 191. [CrossRef]
2. Kianfar, E. Magnetic Nanoparticles in Targeted Drug Delivery: A Review. *J. Supercond. Nov. Magn.* **2021**, *34*, 1709–1735. [CrossRef]
3. Avasthi, A.; Caro, C.; Pozo-Torres, E.; Leal, M.P.; García-Martín, M.L. Magnetic Nanoparticles as MRI Contrast Agents. *Top. Curr. Chem.* **2020**, *378*, 40. [CrossRef]
4. Caspani, S.; Magalhães, R.; Araújo, J.P.; Tavares Sousa, C. Magnetic Nanomaterials as Contrast Agents for MRI. *Materials* **2020**, *13*, 2586. [CrossRef]
5. Stueber, D.D.; Villanova, J.; Aponte, I.; Xiao, Z.; Colvin, V.L. Magnetic Nanoparticles in Biology and Medicine: Past, Present, and Future Trends. *Pharmaceutics* **2021**, *13*, 943. [CrossRef]
6. Kianfar, E. Magnetic Nanoparticles in Medical Imaging. *Imaging Med.* **2022**, *14*, 1–16.
7. Liu, X.; Zhang, Y.; Wang, Y.; Zhu, W.; Li, G.; Ma, X.; Zhang, Y.; Chen, S.; Tiwari, S.; Shi, K.; et al. Comprehensive understanding of magnetic hyperthermia for improving antitumor therapeutic efficacy. *Theranostics* **2020**, *10*, 3793–3815. [CrossRef]
8. Peiravi, M.; Eslami, H.; Ansari, M.; Zare-Zardini, H. Magnetic hyperthermia: Potentials and limitations. *J. Indian Chem. Soc.* **2022**, *99*, 100269. [CrossRef]
9. Aslam, H.; Shukrullah, S.; Naz, M.Y.; Fatima, H.; Hussain, H.; Ullah, S.; Assiri, M.A. Current and future perspectives of multifunctional magnetic nanoparticles based controlled drug delivery systems. *J. Drug Deliv. Sci. Technol.* **2022**, *67*, 102946. [CrossRef]
10. Spoială, A.; Ilie, C.-I.; Motelica, L.; Ficai, D.; Semenescu, A.; Oprea, O.-C.; Ficai, A. Smart Magnetic Drug Delivery Systems for the Treatment of Cancer. *Nanomaterials* **2023**, *13*, 876. [CrossRef] [PubMed]
11. Montiel Schneider, M.G.; Martín, M.J.; Otarola, J.; Vakarelska, E.; Simeonov, V.; Lassalle, V.; Nedyalkova, M. Biomedical Applications of Iron Oxide Nanoparticles: Current Insights Progress and Perspectives. *Pharmaceutics* **2022**, *14*, 204. [CrossRef] [PubMed]
12. Sousa de Almeida, M.; Susnik, E.; Drasler, B.; Taladriz-Blanco, P.; Petri-Fink, A.; Rothen-Rutishauser, B. Understanding nanoparticle endocytosis to improve targeting strategies in nanomedicine. *Chem. Soc. Rev.* **2021**, *50*, 5397. [CrossRef] [PubMed]
13. Haddad, M.; Frickenstein, A.N.; Wilhelm, S. High-throughput single-cell analysis of nanoparticle-cell interactions. *Trac-Trend. Anal. Chem.* **2023**, *166*, 117172. [CrossRef] [PubMed]
14. Ostrowski, A.; Nordmeyer, D.; Boreham, A.; Holzhausen, C.; Mundhenk, L.; Graf, C.; Meinke, M.C.; Vogt, A.; Hadam, S.; Lademann, J.; et al. Overview about the localization of nanoparticles in tissue and cellular context by different imaging techniques. *Beilstein J. Nanotech.* **2015**, *23*, 263–280. [CrossRef] [PubMed]
15. FitzGerald, L.I.; Johnston, A.P.R. It's what's on the inside that counts: Techniques for investigating the uptake and recycling of nanoparticles and proteins in cells. *J. Colloid. Interf. Sci.* **2021**, *587*, 64–78. [CrossRef]
16. Krzyminiewski, R.; Dobosz, B.; Schroeder, G.; Kurczewska, J. ESR as a monitoring method of the interactions between TEMPO-functionalized magnetic nanoparticles and yeast cells. *Sci. Rep.* **2019**, *9*, 18733. [CrossRef]
17. Krzyminiewski, R.; Dobosz, B.; Krist, B.; Schroeder, G.; Kurczewska, J.; Bluyssen, H.A.R. ESR method in monitoring of nanoparticle endocytosis in cancer cells. *Int. J. Mol. Sci.* **2020**, *21*, 4388. [CrossRef]
18. Shashni, B.; Nagasaki, Y. Newly Developed Self-Assembling Antioxidants as Potential Therapeutics for the Cancers. *J. Pers. Med.* **2021**, *11*, 92. [CrossRef]
19. He, W.; Liu, Y.; Wamer, W.G.; Yin, J.-J. Electron spin resonance spectroscopy for the study of nanomaterial-mediated generation of reactive oxygen species. *J. Food Drug Anal.* **2014**, *22*, 49–63. [CrossRef]
20. Suzen, S.; Gurer-Orhan, H.; Saso, L. Detection of Reactive Oxygen and Nitrogen Species by Electron Paramagnetic Resonance (EPR) Technique. *Molecules* **2017**, *22*, 181. [CrossRef]

21. Roessler, M.M.; Salvadori, E. Principles and applications of EPR spectroscopy in the chemical sciences. *Chem. Soc. Rev.* **2018**, *47*, 2534. [CrossRef]
22. Jiang, J.; Tian, S.; Wang, K.; Wang, Y.; Zang, S.; Yu, A.; Zhang, Z. Electron spin resonance spectroscopy for immunoassay using iron oxide nanoparticles as probe. *Anal. Bioanal. Chem.* **2018**, *410*, 1817–1824. [CrossRef] [PubMed]
23. Dogan, N.; Ozel, F.; Koten, H. Structural, Morphological, and Magnetic Characterization of Iron Oxide Nanoparticles Synthesized at Different Reaction Times via Thermal Decomposition Method. *Curr. Nanosci.* **2023**, *19*, 33–38. [CrossRef]
24. Suryawanshi, P.L.; Sonawane, S.H.; Bhanvase, B.A.; Ashokkumar, M.; Pimplapure, M.S.; Gogate, P.R. Synthesis of iron oxide nanoparticles in a continuous flow spiral microreactor and Corning® advanced flow™ reactor. *Green Process. Synth.* **2018**, *7*, 1–11. [CrossRef]
25. Bakker, M.G.; Fowler, B.; Bowman, M.K.; Patience, G.S. Experimental methods in chemical engineering: Electron paramagnetic resonance spectroscopy-EPR/ESR. *Can. J. Chem. Eng.* **2020**, *98*, 1668–1681. [CrossRef]
26. Vasić, K.; Knez, Ž.; Konstantinova, E.A.; Kokorin, A.I.; Gyergyek, S.; Leitgeb, M. Structural and magnetic characteristics of carboxymethyl dextran coated magnetic nanoparticles: From characterization to immobilization application. *React. Funct. Polym.* **2020**, *148*, 104481. [CrossRef]
27. Elamin, N.Y.; Modwi, A.; El-Fattah, W.A.; Rajeh, A. Synthesis and structural of Fe_3O_4 magnetic nanoparticles and its effect on the structural optical, and magnetic properties of novel Poly(methyl methacrylate)/Polyaniline composite for electromagnetic and optical applications. *Opt. Mater.* **2023**, *135*, 113323. [CrossRef]
28. Abele, N.; Münz, F.; Zink, F.; Gröger, M.; Hoffmann, A.; Wolfschmitt, E.-M.; Hogg, M.; Calzia, E.; Waller, C.; Radermacher, P.; et al. Relation of Plasma Catecholamine Concentrations and Myocardial Mitochondrial Respiratory Activity in Anesthetized and Mechanically Ventilated, Cardiovascular Healthy Swine. *Int. J. Mol. Sci.* **2023**, *24*, 17293. [CrossRef]
29. Vanreusel, I.; Vermeulen, D.; Goovaerts, I.; Stoop, T.; Ectors, B.; Cornelis, J.; Hens, W.; de Bliek, E.; Heuten, H.; Van Craenenbroeck, E.M.; et al. Circulating Reactive Oxygen Species in Adults with Congenital Heart Disease. *Antioxidants* **2022**, *11*, 2369. [CrossRef]
30. Velayutham, M.; Poncelet, M.; Eubank, T.D.; Driesschaert, B.; Khramtsov, V.V. Biological Applications of Electron Paramagnetic Resonance Viscometry Using a 13C-Labeled Trityl Spin Probe. *Molecules* **2021**, *26*, 2781. [CrossRef]
31. Gertsenshteyn, I.; Giurcanu, M.; Vaupel, P.; Halpern, H. Biological validation of electron paramagnetic resonance (EPR) image oxygen thresholds in tissue. *J. Physiol.* **2021**, *599*, 1759–1767. [CrossRef]
32. Dobosz, B.; Krzyminiewski, R.; Kucińska, M.; Murias, M.; Schroeder, G.; Kurczewska, J. The spin probes as scavengers of free radicals in cells. *Appl. Sci.* **2022**, *12*, 7999. [CrossRef]
33. Nibbe, P.; Schleusener, J.; Siebert, S.; Borgart, R.; Brandt, D.; Westphalen, R.; Schüler, N.; Berger, B.; Peters, E.M.J.; Meinke, M.C.; et al. Oxidative stress coping capacity (OSC) value: Development and validation of an in vitro measurement method for blood plasma using electron paramagnetic resonance spectroscopy (EPR) and vitamin C. *Free Radic. Biol. Med.* **2023**, *194*, 230–244. [CrossRef]
34. Vesković, A.; Nakarada, Đ.; Pavićević, A.; Prokić, B.; Perović, M.; Kanazir, S.; Popović-Bijelić, A.; Mojović, M. In Vivo/Ex Vivo EPR Investigation of the Brain Redox Status and Blood-Brain Barrier Integrity in the 5xFAD Mouse Model of Alzheimer's Disease. *Curr. Alzheimer Res.* **2021**, *18*, 25–34. [CrossRef]
35. Jakubowska, M.A.; Pyka, J.; Michalczyk-Wetula, D.; Baczyński, K.; Cieśla, M.; Susz, A.; Ferdek, P.E.; Płonka, B.K.; Fiedor, L.; Płonka, P.M. Electron paramagnetic resonance spectroscopy reveals alterations in the redox state of endogenous copper and iron complexes in photodynamic stress-induced ischemic mouse liver. *Redox Biol.* **2020**, *34*, 101566. [CrossRef]
36. Tzivaki, M.; Hassan, A.; Waller, E. Electron paramagnetic resonance spectroscopy for the detection of radiation exposure in dreissenid mussels. *Radiat. Prot. Dosim.* **2023**, *199*, 1626–1631. [CrossRef]
37. Karmakar, P.; Mishra, L.; Mishra, M. Electron spin resonance spectroscopy: A tool for dating mollusc shells, corals, and other materials. In *Spectroscopic and Microscopy Techniques for Archaeological and Cultural Heritage Research*, 2nd ed.; IOP Publishing Ltd.: Bristol, UK, 2023; pp. 9-1–9-11.
38. Timar-Gabor, A.; Kabacińska, Z.; Constantin, D.; Dave, A.K.; Buylaert, J.-P. Reconstructing dust provenance from quartz optically stimulated luminescence (OSL) and electron spin resonance (ESR) signals: Preliminary results on loess from around the world. *Radiat. Phys. Chem.* **2023**, *212*, 111138. [CrossRef]
39. Ghimire, L.; Waller, E. Electron Paramagnetic Resonance Measurements of Lifetime Doses in Teeth of Durham Region Residents, Ontario. *Health Phys.* **2023**, *124*, 175–191. [CrossRef]
40. Cui, X.; Zhang, Z.; Yang, Y.; Li, S.; Lee, C.-S. Organic radical materials in biomedical applications: State of the art and perspectives. *Exploration* **2022**, *2*, 20210264. [CrossRef]
41. Feliciano, C.P.; Nagasaki, Y. Antioxidant Nanomedicine Protects against Ionizing Radiation-Induced Life-Shortening in C57BL/6J Mice. *ACS Biomater. Sci. Eng.* **2019**, *5*, 5631–5636. [CrossRef]
42. Mołoń, M.; Szlachcikowska, D.; Stępień, K.; Kielar, P.; Galiniak, S. Two faces of TEMPO (2,2,6,6-tetramethylpiperidinyl-1-oxyl)—An antioxidant or a toxin? *BBA–Mol. Cell Res.* **2023**, *1870*, 119412. [CrossRef]
43. Feliciano, C.P.; Cammas-Marion, S.; Nagasaki, Y. Recent advances in self-assembling redox nanoparticles as a radiation protective agent. *AIMS Mol. Sci.* **2023**, *10*, 52–69. [CrossRef]
44. Matsumoto, K.-I.; Nakanishi, I.; Zhelev, Z.; Bakalova, R.; Aoki, I. Nitroxyl Radical as a Theranostic Contrast Agent in Magnetic Resonance Redox Imaging. *Antioxid. Redox Signal.* **2022**, *36*, 95–121. [CrossRef]

45. Azuma, R.; Yamasaki, T.; Emoto, M.C.; Sato-Akaba, H.; Sano, K.; Munekane, M.; Fujii, H.G.; Mukai, T. Effect of relative configuration of TEMPO-type nitroxides on ascorbate reduction. *Free Radic. Biol. Med.* **2023**, *194*, 114–122. [CrossRef]
46. Nakamura, H.; Watano, S. Direct Permeation of Nanoparticles Across Cell Membrane: A Review. *Kona Powder Part. J.* **2018**, *35*, 49–65. [CrossRef]
47. Escobar, J.F.; Vaca-González, J.J.; Guevara, J.M.; Garzón-Alvarado, D.A. Effect of magnetic and electric fields on plasma membrane of single cells: A computational approach. *Eng. Rep.* **2020**, *2*, e12125. [CrossRef]
48. Beddoes, C.M.; Case, C.P.; Briscoe, W.H. Understanding nanoparticle cellular entry: A physicochemical perspective. *Adv. Colloid Interfac.* **2015**, *218*, 48–68. [CrossRef]
49. Wen, Z.; Liu, C.; Teng, Z.; Jin, Q.; Liao, Z.; Zhu, X.; Huo, S. Ultrasound meets the cell membrane: For enhanced endocytosis and drug delivery. *Nanoscale* **2023**, *15*, 13532. [CrossRef]
50. Zablotskii, V.; Syrovets, T.; Schmidt, Z.W.; Dejneka, A.; Simmet, T. Modulation of monocytic leukemia cell function and survival by high gradient magnetic fields and mathematical modeling studies. *Biomaterials* **2014**, *35*, 3164–3171. [CrossRef]
51. Min, K.A.; Shin, M.C.; Yu, F.; Yang, M.; David, A.E.; Yang, V.C.; Rosania, G.R. Pulsed magnetic field improves the transport of iron oxide nanoparticles through cell barriers. *ACS Nano* **2013**, *7*, 2161–2171. [CrossRef]
52. Soheilian, R.; Choi, Y.S.; David, A.E.; Abdi, H.; Maloney, C.E.; Erb, R.M. Toward Accumulation of Magnetic Nanoparticles into Tissues of Small Porosity. *Langmuir* **2015**, *31*, 8267–8274. [CrossRef]
53. Zablotskii, V.; Polyakova, T.; Lunov, O.; Dejneka, A. How a High-Gradient Magnetic Field Could Affect Cell Life. *Sci. Rep.* **2016**, *6*, 37407. [CrossRef]
54. Zablotskii, V.; Lunov, O.; Kubinova, S.; Polyakova, T.; Sykova, E.; Dejneka, A. Effects of high-gradient magnetic fields on living cell machinery. *J. Phys. D Appl. Phys.* **2016**, *49*, 493003. [CrossRef]
55. Zablotskii, V.; Lunov, O.; Dejneka, A.; Jastrabik, L.; Polyakova, T.; Syrovets, T.; Simmet, T. Nanomechanics of magnetically driven cellular endocytosis. *Appl. Phys. Lett.* **2011**, *99*, 183701. [CrossRef]
56. Uzhytchak, M.; Lynnyk, A.; Zablotskii, V.; Dempsey, N.M.; Dias, A.L.; Bonfim, M.; Lunova, M.; Jirsa, M.; Kubinová, Š.; Lunov, O.; et al. The use of pulsed magnetic fields to increase the uptake of iron oxide nanoparticles by living cells. *Appl. Phys. Lett.* **2017**, *111*, 243703. [CrossRef]
57. Wang, H.; Zhang, X. Magnetic Fields and Reactive Oxygen Species. *Int. J. Mol. Sci.* **2017**, *18*, 2175. [CrossRef]
58. van der Laan, K.J.; Morita, A.; Perona-Martinez, F.P.; Schirhagl, R. Evaluation of the Oxidative Stress Response of Aging Yeast Cells in Response to Internalization of Fluorescent Nanodiamond Biosensors. *Nanomaterials* **2020**, *10*, 372. [CrossRef]
59. Postaru, M.; Tucaliuc, A.; Cascaval, D.; Galaction, A.-I. Cellular Stress Impact on Yeast Activity in Biotechnological Processes—A Short Overview. *Microorganisms* **2023**, *11*, 2522. [CrossRef]
60. Eigenfeld, M.; Wittmann, L.; Kerpes, R.; Schwaminger, S.; Becker, T. Quantifcation methods of determining brewer's and pharmaceutical yeast cell viability: Accuracy and impact of nanoparticles. *Anal. Bioanal. Chem.* **2023**, *415*, 3201–3213. [CrossRef]
61. Pawlaczyk, M.; Pasieczna-Patkowska, S.; Schroeder, G. Photoacoustic Spectroscopy of Surface-Functionalized Fe_3O_4-SiO_2 Nanoparticles. *Appl. Spectrosc.* **2020**, *74*, 712–719. [CrossRef]
62. Pawlaczyk, M.; Frański, R.; Cegłowski, M.; Schroeder, G. Mass spectrometric investigation of organo-functionalized magnetic nanoparticles binding properties toward chalcones. *Materials* **2021**, *14*, 4705. [CrossRef]
63. Baghdadi, Y.N.; Youssef, L.; Bouhadir, K.; Harb, M.; Mustapha, S.; Patra, D.; Tehrani-Bagha, A.R. Thermal and mechanical properties of epoxy resin reinforced with modified iron oxide nanoparticles. *J. Appl. Polym. Sci.* **2021**, *138*, 50533. [CrossRef]
64. Krzyminiewski, R.; Dobosz, B.; Schroeder, G.; Kurczewska, J. The principles of a new method, MNF-3D, for concentration of magnetic particles in three-dimensional space. *Measurement* **2017**, *112*, 137–140. [CrossRef]
65. Krzyminiewski, R.; Dobosz, B.; Schroeder, G.; Kurczewska, J. Focusing of Fe_3O_4 nanoparticles using a rotating magnetic field in various environments. *Phys. Lett. A* **2018**, *382*, 3192–3196. [CrossRef]
66. Dobosz, B.; Schroeder, G.; Kurczewska, J. Comments on "The principles of a new method, MNF-3D, for concentration of magnetic particles in three-dimensional space". *Measurement* **2023**, *118*, 113146. [CrossRef]
67. Sharpe, M.A.; Baskin, D.S.; Pichumani, K.; Ijare, O.B.; Helekar, S.A. Rotating Magnetic Fields Inhibit Mitochondrial Respiration, Promote Oxidative Stress and Produce Loss of Mitochondrial Integrity in Cancer Cells. *Front. Oncol.* **2021**, *10*, 768758. [CrossRef]
68. Sládičeková, K.H.; Bereta, M.; Misek, J.; Parizek, D.; Jakuš, J. Biological Effects of a Low-Frequency Electromagnetic Field on Yeast Cells of the Genus Saccharomyces Cerevisiae. *Acta Med. Martiniana* **2021**, *21*, 34–41. [CrossRef]
69. Peng, Q.; Huo, D.; Li, H.; Zhang, B.; Li, Y.; Liang, A.; Wang, H.; Yu, Q.; Li, M. ROS independent toxicity of Fe_3O_4 nanoparticles to yeast cells: Involvement of mitochondrial dysfunction. *Chem. Biol. Interact.* **2018**, *1*, 20–26. [CrossRef]
70. Pahlevan, M.; Toivakka, M.; Alam, P. Mechanical properties of TEMPO-oxidised bacterial cellulose-amino acid biomaterials. *Eur. Polym. J.* **2018**, *101*, 29–36. [CrossRef]
71. Chen, L.; Chen, C.; Wang, P.; Song, T. Mechanisms of Cellular Effects Directly Induced by Magnetic Nanoparticles under Magnetic Fields. *Hindawi J. Nanomater.* **2017**, *2017*, 1564634. [CrossRef]